ARTICLES

# Tracing the first stars with fluctuations of the cosmic infrared background

A. Kashlinsky[1,2], R. G. Arendt[1,2], J. Mather[1,3] & S. H. Moseley[1,3]

**The deepest space- and ground-based observations find metal-enriched galaxies at cosmic times when the Universe was less than 1 Gyr old. These stellar populations had to be preceded by the metal-free first stars, known as 'population III'. Recent cosmic microwave background polarization measurements indicate that stars started forming early—when the Universe was ≤200 Myr old. It is now thought that population III stars were significantly more massive than the present metal-rich stellar populations. Although such sources will not be individually detectable by existing or planned telescopes, they would have produced significant cosmic infrared background radiation in the near-infrared, whose fluctuations reflect the conditions in the primordial density field. Here we report a measurement of diffuse flux fluctuations after removing foreground stars and galaxies. The anisotropies exceed the instrument noise and the more local foregrounds; they can be attributed to emission from population III stars, at an era dominated by these objects.**

The cosmic infrared background (CIB) is generated by emission from luminous objects during the entire history of the Universe, including epochs at which discrete objects are inaccessible to current telescopic studies[1,2]. With new powerful telescopes, individual galaxies are now found out to redshifts of $z \gtrsim 5$–7, but the period preceding that of the galaxies seen in the Hubble ultra-deep field remains largely unexplored. These ultra-deep field galaxies and even the highest-$z$ quasars ($z \gtrsim 6.5$) appear to consist of 'ordinary' metal-enriched population I and II stars, suggesting that the metal-free stars of population III existed at still earlier epochs. Large-scale polarization of the cosmic microwave background (CMB)[3] suggests that first stars formed early, at $z \approx 20$.

Current theory predicts that population III objects were very massive stars, with mass greater than 100 solar masses ($100M_{\odot}$; refs 4–6). They should have produced a significant diffuse background[7] with an intensity almost independent of the details of their mass function[8]. Because much of the emission at wavelengths longer than the rest-frame Lyman limit from these epochs is now shifted into the near-infrared (NIR), these stars could be responsible for producing much, or all, of the observed NIR CIB excess over that from normal galaxy populations (see detailed review in ref. 2, and refs 8–13). Two groups[8,13] have recently suggested that this emission should have a distinct angular spectrum of anisotropies, which could be measured if the contributions from the ordinary (metal-rich) galaxies and foregrounds could be isolated and removed, and provide an indication of the era made predominantly of the massive population III stars.

Measuring CIB anisotropies from objects at high $z$ is difficult, because the spatial fluctuations are small and can be hidden by the contributions of ordinary low-$z$ galaxies as well as instrument noise and systematic errors in the data. Previous attempts to measure the structure of the CIB in the NIR on the degree scale with COBE/DIRBE[14] and IRTS/NIRS[15] were limited in sensitivity because of the remaining contributions from brighter galaxies in the large beams. Analysis of 2MASS data at 1.25, 1.65 and 2.2 μm with ~2 arcsec resolution[16,17] allowed removal of foreground galaxies to a K magnitude of 19–19.5 (AB magnitude $m_{AB} \approx 21$ or 15 μJy), and led to measurements of CIB fluctuations at 1.25 to 2.2 μm at sub-arcminute angular scales. These studies reported fluctuations in excess of that expected from the observed galaxy populations, although their accurate interpretation in terms of high-$z$ contributions is difficult owing to foreground galaxies and non-optimal angular scales.

We used data from deep exposure data obtained with Spitzer/IRAC[18,19] in four channels (channels 1–4 correspond to wavelengths of 3.6, 4.5, 5.8 and 8 μm, respectively) in attempting to uncover this signal. We find significant CIB anisotropies after subtracting galaxies substantially fainter than was possible in prior studies, that is, down to $m_{AB} \approx 22$–25. The angular power spectrum of the anisotropies is significantly different from that expected from Solar System and Galactic sources, its amplitude is much larger than what is expected from the remaining faint galaxies, and can reasonably be attributed to the diffuse light from the population III era.

## Assembly and reduction of data sets

The primary data set that we used here is the deep IRAC observation of a $\sim 12' \times 6'$ region around the quasi-stellar object (QSO) HS 1700+6416 obtained by the Spitzer instrument team[18,20]. In addition, the data from two auxiliary fields with shallower exposures (HZF and EGS) were analysed. Relevant data characterizing the fields are listed in Table 1. For this analysis, the raw data were reduced using a least-squares self-calibration method[21]; the processing is described in more detail in Supplementary Information.

The random noise level of the maps was computed from two subsets (A, B) containing the odd- and even-numbered frames, respectively, of the observing sequence. The A and B subsets were observed nearly simultaneously and with similar dither patterns and exposures. The difference between maps generated from the A and B subsets should eliminate true celestial sources and stable instrumental effects, and reflect only the random noise of the observations.

Analysis of the background fluctuations must be preceded by steps that eliminate the foreground Galactic stars and the galaxies bright enough to be individually resolved. The primary means of removing these sources is an iterative clipping algorithm which zeroes all pixels (and a fixed number of neighbouring pixels, $N_{mask} \times N_{mask}$) that are more than a chosen factor, $N_{cut}$, above the $1\sigma$ r.m.s. variation in the clipped surface brightness. This must be restricted to relatively high

[1]Observational Cosmology Laboratory, [2]SSAI, [3]NASA, Code 665, Goddard Space Flight Center, Greenbelt, Maryland 20771, USA.

**Table 1 | Details of analysed fields**

| Region | QSO 1700 (Ch. 1–4) | HZF (Ch. 1–3) | HZF (Ch. 4) | EGS (Ch. 1–4) |
|---|---|---|---|---|
| $(\alpha, \delta)$ | (255.3, 64.2) | (136.0, 11.6) | (285.7, −17.6) | (215.5, 53.3) |
| $(l, b)_{Gal}$ | (94.4, 36.1) | (217.5, 34.6) | (18.4, −10.4) | (96.5, 58.9) |
| $(\lambda, \beta)_{Ecl}$ | (194.3, 83.5) | (135.0, −4.9) | (285.0, 5.0) | (179.9, 60.9) |
| $\langle t_{obs} \rangle$ (*h*) | 7.8, 7.8, 7.8, 9.2 | 0.5, 0.5, 0.5 | 0.7 | 1.4, 1.4, 1.4, 1.4 |
| $m_{Vega,lim}$ | 22.5, 20.5, 18.25, 17.5 | 21.5, 19.5, 17 | 14.5 | 22.5, 20.75, 18.5, 17.75 |
| Pixel scale (″) | 0.6 | 1.2 | 1.2 | 1.2 |
| Field size (pix) | 1,152 × 512 | 576 × 256 | 576 × 256 | 640 × 384 |

QSO 1700 was observed during In-Orbit Checkout (IOC) with eight AORs (Astronomical Observation Requests), which used various dither patterns and 200-s frame times, except for two which used 100-s frame times (AOR ID numbers = 7127552, 7127808, 7128064, 7128320, 7128576, 7475968, 7476224, 7476480). Because of the focal plane offset between the shared 3.6/5.8 μm and 4.5/8 μm fields of view, each of these pairs observes separate fields that have a common overlap of ~5′ × 5′ at all four wavelengths. To provide contrast for the self-calibration algorithm, data from a high-zodiacal light brightness field (HZF) was co-processed for each channel. For 3.6, 4.5 and 5.8 μm, the nearest suitable (200-s frame time) data were observed later during IOC (AOR ID number = 8080896). For the 8-μm data, because nominal 100- and 200-s frame times are split into pairs and quartets of 50-s frames, more nearly contemporaneous observations earlier during IOC were used (AOR ID number = 6849280). For this work we only self-calibrated the six 200-s AORs for 3.6–5.8 μm, but at 8 μm all eight AORs were used as all produce data with 50-s frame times. Observations of the extended Groth Strip area (EGS) provide an additional deep data set for verification of our results. Separate exposure times and limiting magnitudes apply for channels 1–4 respectively. $(a,\delta)$ are right ascension and declination, $(l,b)$ and $(\lambda,\beta)$ are Galactic and Ecliptic (longitude, latitude) respectively. All coordinates are in degrees. $\langle t_{obs} \rangle$ is the mean integration time in hours. The maps for the main QSO 1700 field are shown in Supplementary Information.

$N_{cut}$ to leave enough area for a robust Fourier analysis of the map, and to avoid clipping into the background fluctuation distribution. This means that faint sources, the faint outer portions of resolved galaxies, and the faint wings of the point source response function around bright stars cannot be clipped adequately. To remove these low surface brightness sources, we used a CLEAN algorithm[22] to model the entire field in each channel. This model, convolved with the full IRAC point spread function, was subtracted from the unclipped regions of the map. Supplementary Information provides details on this process and illustrations of the clipped and model-subtracted images. The final step is the fitting and removal of the zeroth- and first-order components of the background in the unclipped regions. This is done to minimize power spectrum artefacts due to the clipping, and because the lack of an absolute flux reference measurement and observing constraints prohibit unambiguous determination of these components. With this subtraction, the images represent the fluctuation fields, $\delta F(\mathbf{x})$, at position $\mathbf{x}$ rather than the absolute intensity $F$. For each observed field, these steps were carried out for images derived from the full data set and from the A and B subsets.

## Power spectrum computation and analysis

For each channel, we calculate the power spectra of the fluctuations as a quantitative means of characterizing their scale and amplitude.

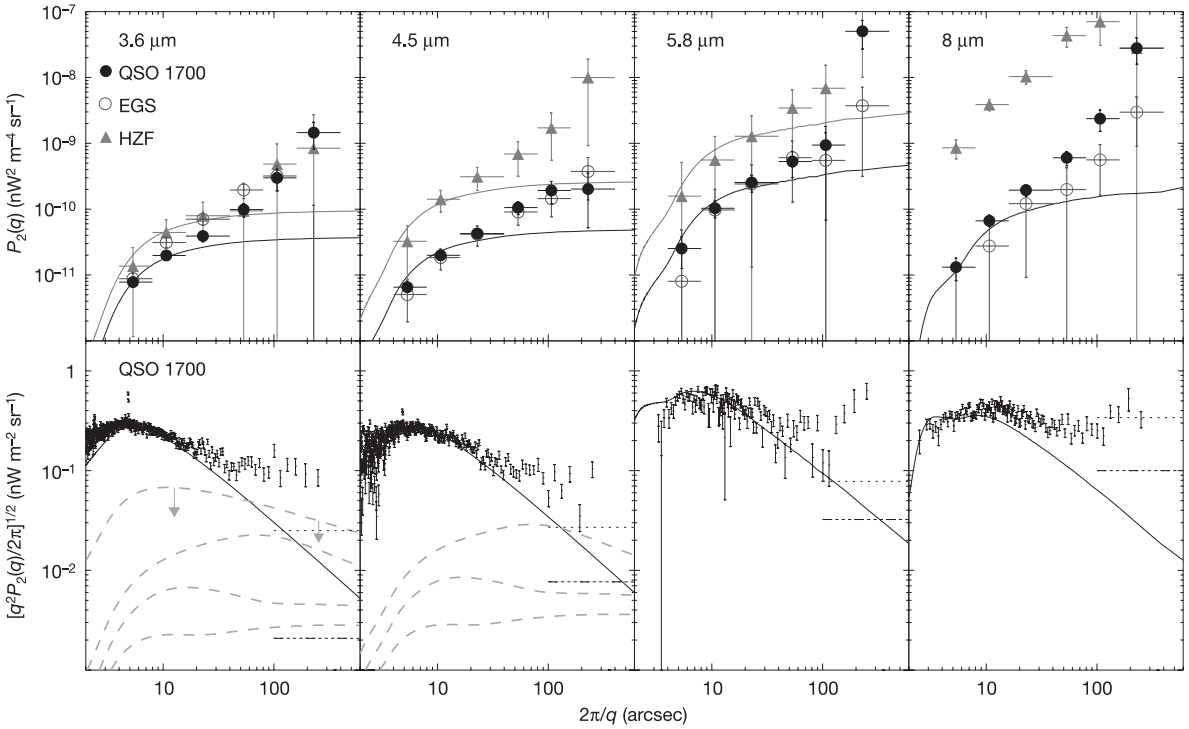


**Figure 1 | Spectra of CIB fluctuations.** Top, power spectra of signal minus noise from Supplementary Fig. 2 averaged over wide bins to increase signal-to-noise ratio. The errors are $N_q^{-1/2}$, corresponding to the cosmic variance, where $N_q$ is the number of Fourier elements at the given $q$-bin. Solid lines show the shot noise from remaining galaxies fainter than the limiting magnitude in Table 1. Filled circles and the darkest shade error bars correspond to the QSO 1700 data, open circles and intermediate shade error bars to the EGS data, and triangles with the lightest shade error bars and lines correspond to HZF data. Bottom panels, fluctuations, $[q^2P(q)/2\pi]^{1/2}$, versus $2\pi/q$ (see text) for the QSO 1700 data. Dashed lines estimate the contribution from ordinary galaxy populations and ΛCDM density field with $\Delta t = 5$ Gyr: the top dashed line shows the upper limit, which assumes that their (high-$z$) clustering pattern remained identical to that today at $z = 0$ and the other dashed lines correspond to $\langle z \rangle = 1, 3, 5$ from top to bottom. Solid lines show shot noise from remaining ordinary galaxies. Dotted and dash-dot-dotted lines show the estimated Galactic cirrus and zodiacal light contributions, respectively, assuming the power spectra to be $P(q) \propto q^n$ with $n = -2$, typical of cloud distributions. The observed cirrus power spectrum is a little steeper with $n \approx -2.5$ to $-3$ (refs 14, 37, 38, 39) in which case the lines will have a slope of $(3 + n)/2 = 0.25$ to 0.5.

**Table 2 | Cross-correlation coefficients of fluctuations**

| Channels | $N_{cut} = 4$ | $N_{cut} = 2$ |
|---|---|---|
| 1: 2 | 52 | 12 |
| 1: 3 | 7 | 0.6 |
| 1: 4 | 10 | 4 |

The cross-correlation coefficients are shown for various clipping thresholds and are in units of that of random sample $\mathcal{R}/\sigma_{\mathcal{R}}$. These correlations were evaluated for an evenly covered region of $512^2$ pixels common to all four channels for the QSO 1700 field. For random uncorrelated samples, $\delta_1$, $\delta_2$, of $N_{pixels}$, the correlation coefficient, $\mathcal{R} \equiv \langle\delta_1\delta_2\rangle/[\langle\delta_1^2\rangle\langle\delta_2^2\rangle]^{1/2}$, should be zero with dispersion $\sigma_{\mathcal{R}} = N_{pixels}^{-1/2}$. In fact, for $N_{mask} = 3$, we find that down to even $N_{cut} = 2$, when only 6% of the pixels remain, the correlations between the channels remain statistically significant. Simple simulations containing the appropriate levels of the instrument noise and a power law component of the CIB gave somewhat larger mean values of $\mathcal{R}$ with the measured values lying within a 95% confidence level; incorporating the possibility that not all of the remaining ordinary galaxies are the same at each wavelength would, however, reduce the mean values of $\mathcal{R}$.

The power that remains after subtraction of the random noise component is insensitive to the details of the source clipping, and is statistically correlated between channels. This confirms that the fluctuation signal does have a celestial origin. The shape and amplitude of the power spectra are not consistent with significant contributions from the cirrus of the interstellar medium (except perhaps at 8 μm) or from the zodiacal light from local interplanetary dust.

The fluctuation field, $\delta F(\mathbf{x})$, was weighted by the observation time $t_{obs}$ in each pixel, $w(\mathbf{x}) \propto t_{obs}(\mathbf{x})$, and its Fourier transform, $f(\mathbf{q}) = \int \delta F(\mathbf{x}) w(\mathbf{x}) \exp(-i\mathbf{x}\cdot\mathbf{q}) d^2x$ as function of the angular wavenumber $\mathbf{q}$ calculated using the fast Fourier transform. (The weighting is necessary to minimize the noise variations across the image, but we also performed the same analysis without it and verified that the weight adds no structure to the resultant power spectrum. This is because the weights are relatively flat across the image.) The power spectrum is $P_2(q) = \langle|f(\mathbf{q})|^2\rangle$, with the average taken over all the Fourier elements $N_q$ corresponding to the given $q$. A typical flux fluctuation is $\sqrt{q^2P_2(q)/2\pi}$ on the angular scale of wavelength $2\pi/q$. In the Supplementary Information we show the final power spectrum of the diffuse flux fluctuations, $P_S(q)$, and the noise, $P_N(q)$, of the data sets. We find significant excess of the large-scale fluctuations over the instrument noise.

Figure 1 shows the excess power spectrum, $P_S(q) - P_N(q)$, of the diffuse light after the instrument noise has been subtracted at 3.6, 4.5, 5.8 and 8 μm. The errors correspond to standard deviation for the cosmic variance, i.e. the relative error on each $P_S(q)$, $P_N(q)$ is $N_q^{-1/2}$. There is a clear positive residual whose power spectrum is significantly different from white noise and has substantial correlations all the way to the largest scales probed. Possible sources of these large-scale correlations can be artefacts of the analysis procedure (such as clipping and fast Fourier transforms), instrumental artefacts, local Solar System or Galactic emission, or relatively nearby extragalactic sources and/or more distant cosmological sources. In what follows we discuss their relative contributions.

Residual emission from the wings of incompletely clipped sources can give rise to spurious fluctuations, but the power spectrum of these fluctuations should depend on the clipping parameters $N_{cut}$ and $N_{mask}$. We tested the contributions from these residuals in various ways. For a given $N_{cut}$ we varied $N_{mask}$ from 3 to 7, significantly reducing any residual wings and increasing the fraction of the clipped pixels, but found negligible (less than a few per cent) variations in the final $P_2(q)$. We also clipped down to progressively lower values of $N_{cut}$. For $N_{cut} \lesssim 3.5$, too few pixels remain for robust Fourier analysis, so in these cases we computed $C(\theta)$, the correlation function of the diffuse emission, as a function of angular separation $\theta$, related to the power spectrum by a one-dimensional Legendre transformation. It is consistent with the fluctuations in Fig. 1 as discussed and shown in Supplementary Information.

Instrument noise contributions to the fluctuations were evaluated as the power spectra of $\frac{1}{2}(\delta F_A - \delta F_B)$ using the A−B subset images. As shown in the Supplementary Information, random instrument noise has an approximately white spectrum. The power spectra of the final data sets have a much larger amplitude than the noise (especially in channels 1 and 2) until the convolution with the beam tapers off the signals from the sky at the smallest angular scales. The instrument noise spectra are unaffected by the beam and are uncorrelated from channel to channel, as expected. However, the full data set fluctuation fields show statistically significant correlations between channels, as shown in Table 2. This means that we see the same fluctuation field in addition to (different) noise in all four channels. In Supplementary Information we describe tests to assess the contributions of possible instrumental systematic errors. They indicate that systematic instrumental effects are unlikely to lead to the signal shown in Fig. 1.

The best assessment of zodiacal light contributions to the power spectrum comes from the examination of EGS observations taken at two epochs six months apart. Because any anisotropies in the zodiacal light cloud will not remain fixed in celestial coordinates over this interval, the difference in the fluctuation fields at these two epochs should eliminate Galactic and extragalactic signals and yield a power spectrum of the zodiacal light fluctuations added to the instrument noise and possible systematic errors. The fluctuation levels of these difference maps set an upper limit on the zodiacal light contribution of $<0.1\,\mathrm{nW\,m^{-2}\,sr^{-1}}$ at 8 μm. Scaling this result to the other channels by interpolating the observed zodiacal light spectrum[23] leads to zodiacal light contributions to the fluctuations that are comfortably below the detections in Fig. 1 in the other channels as well.

Our assessment of the contribution of the infrared cirrus (that is, interstellar clouds of neutral gas and dust) to the power spectra is derived from the 8 μm HZF field, which lies at low Galactic latitude and is visibly contaminated by cirrus. Assuming that the large-scale fluctuations in this field are due to the cirrus, relative fluctuations of the 8 μm cirrus are ∼1% of the mean cirrus flux level. A similar level of relative cirrus fluctuations in the QSO 1700 field would have an amplitude of $\sim 0.3\,\mathrm{nW\,m^{-2}\,sr^{-1}}$. This is not significantly lower than the 8 μm amplitude observed in Fig 1. Therefore, we cannot at present eliminate the possibility that the fluctuations at 8 μm are dominated by cirrus. However, the spectrum of the interstellar medium emission should drop sharply at shorter wavelengths as the PAH (polycyclic aromatic hydrocarbons) emission bands that dominate at 8 μm become less significant. Given this estimate of the cirrus contribution at 8 μm we estimate the amplitude of large-scale fluctuations for channels 1–3 as ∼0.03, 0.03 and $0.08\,\mathrm{nW\,m^{-2}\,sr^{-1}}$,

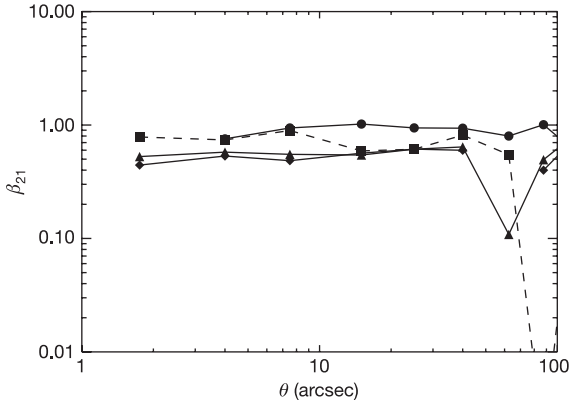


**Figure 2 | Colour properties of clipped maps.** Estimates of colour between channels 1 and 2. Circles correspond to $\sqrt{P_2/P_1}$, averaged over the bins centred at these angles, diamonds to $\langle\delta F_2(x)\delta F_1(x+\theta)\rangle/\langle\delta F_1(x)\delta F_1(x+\theta)\rangle$ for $N_{cut} = 4$, and triangles to the same quantity averaged over maps with $N_{cut} = 4, 3, 2.5, 2$. Squares correspond to $\beta_{41}/\beta_{42}$ averaged over maps with $N_{cut} = 4, 3, 2.5, 2$. (See text for definitions of variables.)

which are well below the observed fluctuations in these channels.

Colour is another important criterion for testing the origins of the signal in Fig. 1. The cross-correlations between the channels for the common area of the QSO 1700 field are statistically significant and they also strengthen at the larger scales where the noise contribution is smaller, as verified by smoothing the maps. These significant cross-correlations allow us to examine the corresponding colours of the fluctuations. We made several estimates of the colours, $\beta_{n1}$, between channels $n$ and 1: first, as the square root of ratio of the power spectra, and second, as $\beta_{n1}(\theta) = \langle \delta F_n(x)\delta F_1(x+\theta)\rangle / \langle \delta F_1(x)\delta F_1(x+\theta)\rangle$ evaluated over the $512^2$ pixel field common to all four channels, where a further consistency check comes from comparison between $\beta_{21}$ and $\beta_{41}/\beta_{42}$. For channels 1 and 2 these estimates are shown in Fig. 2, and appear roughly independent of angular scale and mutually consistent. The instrument noise is too large to enable robust colour estimates involving channel 3 (5.8 μm). These derived colours indicate that the fluctuation signal in Fig. 1 has an energy distribution that is approximately flat to slowly rising with wavelength in $\nu I_\nu$, where $I_\nu$ is intensity at frequency $\nu$. The energy spectrum rules out contributions from remaining Galactic stars, but probably cannot be used to distinguish between ordinary galaxies and population III objects without additional detailed modelling of both sets of sources.

## CIB fluctuations from extragalactic sources

There are two extragalactic classes of contributors to CIB fluctuations: 'ordinary' galaxies containing normal stellar populations I and II, and the objects that preceded them, population III stars. The square of the CIB fluctuation in band $\nu$ produced by cosmological sources that existed over time period $\Delta t$ is given by the power-spectrum version of the Limber equation (see ref. 2 and Supplementary Information):

$$\frac{q^2 P_2(q)}{2\pi} = \Delta t \int \left(\frac{\mathrm{d}I_{\nu'}}{\mathrm{d}t}\right)^2 \Delta^2(q d_A^{-1}; z)\mathrm{d}t \qquad (1)$$

where $\nu' = \nu(1+z)$ is the rest frequency of the emitters, $d_A$ is the comoving angular diameter distance, and

$$\Delta(k) = \sqrt{\frac{1}{2\pi}\frac{k^2 P_3(k)}{c\Delta t}} \qquad (2)$$

is the fluctuation in the number of sources within a volume $k^{-2}c\Delta t$ and $k$ is the spatial wavenumber. The fluctuation of the CIB with mean flux $F_{\mathrm{CIB}}$ on angular scale $\sim 2\pi/q$ can then be expressed as $\delta F_{\mathrm{CIB}} = F_{\mathrm{CIB}}\Delta(q d_A^{-1}(\langle z\rangle))$, where $\langle z\rangle$ is the suitably averaged effective redshift. The relative CIB fluctuation is the suitably averaged fluctuation in the source counts over a cylinder of radius $q^{-1}d_A(\langle z\rangle)$ and length $c\Delta t$. Three things would lead to larger fluctuations; (1) a population that, after removing constituents brighter than some limit, leaves a substantial mean CIB flux (increase $F_{\mathrm{CIB}}$), (2) populations that existed for a shorter time (increase $\langle\Delta\rangle$ by decreasing $\Delta t$), and (3) populations that formed out of rare peaks of the underlying density field leading to biased and significantly amplified[24], clustering properties (increase $\langle\Delta\rangle$ by increasing $P_3(k)$).

## CIB fluctuations from remaining ordinary galaxies

The fluctuations produced by ordinary galaxies contain two components: first, shot noise from discrete galaxies, and second, galaxy clustering from the primeval density field. The amplitude of the first component can be estimated directly from galaxy counts. In order to estimate the contribution from the second component we proceed as follows: from galaxy count data we estimate the total CIB flux produced by the remaining galaxies fainter than our clipping threshold. Ordinary galaxies occupy an era of $\Delta t \gtrsim$ a few Gyr. Their present-day clustering pattern on the relevant scales is well measured today. The clustering pattern evolution can be extrapolated to earlier times assuming the 'concordance' ΛCDM model (see below). These parameters (flux, $\Delta t$, clustering pattern and its evolution) then allow us to estimate the contribution to the CIB fluctuations via equations (1) and (2). Because galaxy clustering is weaker at earlier times, an upper limit on the contribution from ordinary galaxies is obtained assuming that the clustering at early times remained the same as at $z = 0$.

The shot noise component contributed by the ordinary galaxies to the CIB angular spectrum was estimated directly from galaxy count data: each magnitude bin $\Delta m$ with galaxies of flux $f(m)$ would contribute a power spectrum of $P_{\mathrm{sn}} = f^2(m)\frac{\mathrm{d}N_{\mathrm{gal}}}{\mathrm{d}m}\Delta m$. Figure 1 shows the shot noise component convolved with the IRAC beam for the galaxies at the limiting magnitude in Table 1. The limiting magnitudes are qualitative estimates of where the SExtractor[25] number counts (in 0.5 magnitude bins) begin to drop sharply due

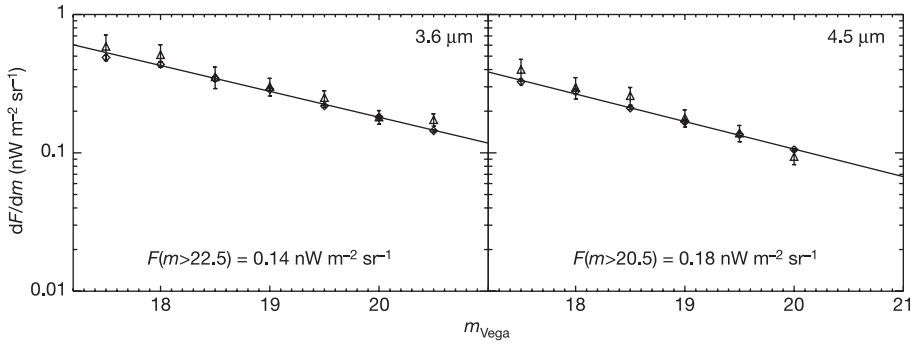


**Figure 3 | Contribution to CIB flux from Spitzer IRAC galaxy counts at 3.6 μm and 4.5 μm.** Vertical axis shows the flux, $F$, produced by galaxies in the magnitude range $[m, m + \mathrm{d}m]$ shown on the horizontal axis. Errors correspond to standard deviation in poissonian number counts. The value of $\mathrm{d}F/\mathrm{d}m$ is evaluated from counts data and is a rapidly decreasing function of $m$ of the form $\mathrm{d}F/\mathrm{d}m \propto \exp(bm)$ with $b \approx 0.4$ (the least squares fits are shown with solid lines). (At the other two IRAC channels the uncertainty in the fall-off is much greater, but we show below that definite conclusions can already be reached from the data at 3.6 and 4.5 μm). Assuming that the functional form of $\mathrm{d}F/\mathrm{d}m$ does not begin to rise appreciably at still fainter magnitudes gives the CIB contribution from galaxies fainter than $m_0$ of $F(m > m_0) = b^{-1}\mathrm{d}F/\mathrm{d}m|_{m_0}$. For the QSO 1700 field, we eliminate galaxies brighter than $m_{\mathrm{Vega}} \approx 22.5$ at 3.6 μm and $m_{\mathrm{Vega}} \approx 20.5$ at 4.5 μm corresponding to AB magnitudes ~25 and 24, respectively. The annotation in each panel shows numbers that correspond to the extrapolated total flux from galaxies fainter than the magnitude limits in Table 1 using the least-squares fits shown with solid lines. One can expect that galactic spectra at the appropriate range of wavelengths are at most as steep as that of Vega, a star with a Rayleigh-Jeans black body spectral fall-off at these wavelengths. If so, they would generally have $K - m_{3.6} > 0$, leaving galaxies with $K \gtrsim 22$ (see, for example, ref. 40). Galaxies at K >20 have median redshift $\gtrsim 1$ (ref. 41), so the above argument would place the galaxies remaining at 4.5 μm at $z \gtrsim 1$ and those remaining at 3.6 μm still farther out to higher $z$. Comparison with the Lyman-break galaxy candidates in the same area shows that a substantial fraction of these galaxies are at $z \approx 2$–4, with $z \sim 3$ being the median redshift[20]. Similarly, a substantial part of these galaxies are confirmed to be star-forming systems at $z \approx 2.3$ (ref. 42).

to incompleteness. The shot noise fits the observed diffuse light fluctuations well at small angles, but the shot-noise contribution from ordinary galaxies cannot make a substantial contribution to the large-scale power of the diffuse light in Fig. 1.

We assume the 'concordance' ΛCDM model Universe with flat geometry (total density parameter $\Omega_{\rm total} = 1$) dominated by a cosmological constant, $\Omega_\Lambda \approx 0.7$, with the rest coming from cold dark matter and ordinary baryons in proportions suggested by measurements of the CMB anisotropies[26] and high-$z$ supernovae[27]. With $P_3(k)$ taken from the ΛCDM concordance model, the power in fluctuations from the clustering of ordinary galaxies depends on the net flux produced by the remaining ordinary galaxies (via $F_{\rm CIB}$) and their typical redshifts (via $\Delta(qd_A^{-1})$). The total flux from galaxies fainter than the limiting magnitude in Table 1 was estimated from the Spitzer IRAC galaxy counts[18], and is shown in Fig. 3. The flux contributed to the CIB from the remaining galaxies is between 0.1 and 0.2 nW m$^{-2}$ sr$^{-1}$ and this amplitude is much less than the excess CIB at these wavelengths[2] indicating that the excess CIB flux is produced by populations that are still farther out than the ordinary galaxies remaining in the data. This (low) value of the remaining flux can also be derived from the small amplitude of the residual shot-noise contribution to the fluctuations in the confusion-limited data sets. Thus, in order to explain the amplitudes shown in Fig. 1, the remaining ordinary galaxy populations would need to produce relative flux fluctuations of the order of $\gtrsim 100\%$ from their clustering. Without follow-up spectroscopy it is difficult to determine with high precision the range of redshifts of the remaining ordinary galaxies, but approximate estimates can be made, and are summarized in the Fig. 3 legend to be $z \gtrsim 1$.

In flat cosmology with $\Omega_\Lambda = 0.7$, one arcminute subtends a comoving scale between 0.7 and $1.6\,h^{-1}$ Mpc at $z$ between 1 and 5. The present-day three-dimensional power spectrum of galaxy clustering, $P_{3,\rm gal}(k)$, is described well by the concordance ΛCDM model[28,29] and we expect that on arcminute scales the density field was in the linear to quasi-linear regime at the redshifts probed by the remaining galaxies between 3.6 and 8 μm. At smaller scales, nonlinear corrections to evolution were computed following ref. 30. The resultant CIB fluctuation from the remaining ordinary galaxies, producing mean CIB $F_{\rm CIB,og} = 0.14$ nW m$^{-2}$ sr$^{-1}$, times $\Delta(\propto(\Delta t)^{-1/2})$ is shown in Fig. 1 for $\langle z\rangle = 1$, 3, 5 and $\Delta t = 5$ Gyr, corresponding to the age of the Universe at $z \approx 1$. For the ΛCDM model, the relative fluctuations in the CIB on arcminute scales would be of the order of $\langle\Delta\rangle \approx (2-10)\times 10^{-2}(\Delta t)^{-0.5}$ from galaxies with $\langle z\rangle = 1$–5 assuming no biasing (here $\Delta t$ is in units of 5 Gyr). Combining this with the above values for the diffuse flux from the remaining ordinary galaxies would lead to $\delta F \lesssim (1\text{–}2)\times 10^{-2}$ nW m$^{-2}$ sr$^{-1}$ in all the channels. While biasing may increase the relative fluctuations, with reasonable bias factors for galaxies lying at $z \approx$ (a few), the diffuse light fluctuations would still be very small compared to those in Fig. 1 and are unlikely to account for fluctuations of amplitude ~(0.1–0.5) nW m$^{-2}$ sr$^{-1}$ at arcminute scales. An upper limit on the CIB fluctuations can be evaluated assuming the same clustering pattern for the remaining galaxies as at the present epoch, $z = 0$, that is, that their two-point correlation function is given by $\xi = (r/r_\star)^{-1.7}$ with $r_\star = 5.5h^{-1}$ Mpc (ref. 31); its $\Delta$ times $F_{\rm CIB,og}$ is also shown in Fig. 1 and is much below the signal we measure. Conversely, one can evaluate the clustering strength needed to account for the observed fluctuations: a 100% relative fluctuation from galaxies at $z \gtrsim 1$ clustered with $\xi = (r/r_\star)^{-1.7}$ would require $r_\star \gtrsim 25h^{-1}$ Mpc. This corresponds to the effective bias factor $\gtrsim 5$, which is significantly higher than expected from gravitational clustering evolution in the ΛCDM universe[32]. In fact, direct measurements of clustering for relatively nearby IRAC galaxies with flux >32 μJy at 3.6 μm (~5 mag brighter than the limit reached for remaining galaxies in the QSO 1700 field)[33] find the projected two-point correlation amplitude on ~arcminute scales of $w_{>32\,\mu\rm Jy}(\theta \gtrsim 1') < 4\times 10^{-2}$ corresponding to relative fluctuations in CIB from these galaxies of amplitude $\sim\sqrt{w} \lesssim 0.2$. Fainter galaxies are expected to have an even lower correlation amplitude.

The QSO 1700 field seems to contain an overdensity of Lyman-break galaxies at $z \approx 2.3$ (ref. 34) which could lead to a larger $\Delta$ and CIB fluctuations for this region. However, we see similar levels of fluctuations for the other fields located at very different parts of the sky, making it unlikely that the overdensity claimed in ref. 34 can account for our signal. When account is made of the different shot noise levels from the remaining galaxies, the fluctuations seen in the different fields have consistent power spectra within the statistical uncertainties. (An exception is channel 4 HZF data, located at low Galactic Latitude, and clearly dominated by Galactic cirrus.)

### CIB fluctuations from the population III era

Population III objects at $z \approx$ 10–30 are expected to precede ordinary galaxy populations. One can expect on fairly general grounds[8] that, if massive, they would contribute significantly to the NIR CIB, in terms of both its mean level and anisotropies. Intuitive reasons are discussed in ref. 2, but as equations (1) and (2) show, they are mostly related to: (1) if massive, population III were very efficient light emitters, (2) their era probably lasted a shorter time, $\Delta t$, than that of the ordinary galaxies, leading to larger $\Delta$ in equation (2), and (3) they should have formed out of high peaks of the density field whose correlation function is strongly amplified. The NIR also probes ultraviolet to visible parts of the electromagnetic spectrum at $z \approx$ 10–30, where most of their emission is produced[12].

The amplitude of the CIB anisotropies remaining in the present data implies that the remaining CIB originates from still fainter objects. Can the observed amplitudes of fluctuations in Fig. 1 be accounted for by energetic sources at high $z$? Population III stars can produce significant NIR CIB levels[12], $\gtrsim 1$ nW m$^{-2}$ sr$^{-1}$ and, for example, the NIR CIB excess over that from ordinary galaxies at 3.6 μm is $8.7 \pm 3.1$ nW m$^{-2}$ sr$^{-1}$ (ref. 2). At other NIR wavelengths >1 μm, the mean NIR CIB excess is also more than a few nW $^{-2}$ sr$^{-1}$ (refs 15, 43–49). Thus population III objects would require smaller relative CIB fluctuations. Because individual population III systems are small, yet numerous, the shot-noise component of the CIB from them is small and, in any case, is already absorbed in the shot-noise shown in Fig. 1. Additionally, their $\langle\Delta\rangle$ would be amplified by the much shorter $\Delta t$ and (significant) biasing, and population III contribution would dominate the diffuse light fluctuations in Fig. 1. Detailed theoretical interpretation of the results in terms of the population III era models exceeds the scope of this Article, but qualitative comparison can be made by estimating the typical value of the relative CIB fluctuation, $\Delta$, corresponding to that era. The fraction of the population III haloes was calculated assuming that they form from the ΛCDM density field in haloes where the virial temperature $T_{\rm vir} \geq 2{,}000$ K to enable efficient molecular hydrogen cooling[35]. Biasing was treated using the gravitational clustering prescription from ref. 36 in the ΛCDM model. (Nonlinear evolution effects are small on the angular scales and redshifts probed here.) Assuming $\Delta t \approx 300$ Myr, which corresponds to the age of the Universe at $z = 0$, we get typical values of $\Delta \approx$ 0.1–0.2 at $z$ between 10 and 20. This order-of-magnitude evaluation shows that the levels of ~0.1–0.3 nW m$^{-2}$ sr$^{-1}$ at 3.6 to 8 μm on arcminute scales can be accounted for by population III emissions if their total flux contribution is >1 nW m$^{-2}$ sr$^{-1}$, which is reasonable, as discussed earlier.

Earlier studies of CIB fluctuations[14–16] contained significant contributions from relatively bright galaxies, making it difficult to isolate the possible CIB fluctuations from the very early times. The contribution to CIB fluctuations from remaining galaxies is a function of the limiting magnitude below which galaxies are removed. With the Spitzer IRAC data we could identify and remove galaxies to very faint limits of flux $\gtrsim$0.3 μJy. This limit is, at last, sufficiently low to push the residual contribution from ordinary galaxies along the line-of-sight below the level of the excess signal at larger angular scales. If our

interpretation is correct and the signal we detect comes from population III located at much higher $z$, the amplitude of the CIB fluctuations on scales where galaxy shot-noise is negligible should remain the same as fainter ordinary galaxies are removed with deeper clipping. This is true as far as we can test with this data, and would certainly be verifiable with longer-exposure data.

At these $z$ the IRAC bands probe the rest-frame wavelengths between 0.2 and 0.8 μm, where the energy spectra of individual population III objects is dominated by free-free emission and is a slowly rising function of wavelength[12]; this would be consistent with the spectrum of the CIB anisotropies in Fig. 1. NIR observations at shorter wavelengths would be particularly important in confirming the redshifts where the CIB fluctuations originate, as there should be a significant drop in the power of the fluctuations at the rest-frame Lyman limit wavelength.

**Received 3 May; accepted 12 August 2005.**


1. Hauser, M. G. & Dwek, E. The cosmic infrared background: Measurements and implications. *Annu. Rev. Astron. Astrophys.* **39,** 249–307 (2001).
2. Kashlinsky, A. Cosmic infrared background and early galaxy evolution. *Phys. Rep.* **409,** 361–438 (2005).
3. Kogut, A. *et al.* First year Wilkinson Microwave Anisotropy Probe (WMAP) observations: Temperature-polarization correlation. *Astrophys. J. Suppl.* **148,** 161–173 (2003).
4. Abel, T. *et al.* The formation of the first star in the Universe. *Science* **295,** 93–98 (2002).
5. Bromm, V. *et al.* Forming the first stars in the Universe: The fragmentation of primordial gas. *Astrophys. J.* **527,** L5–L8 (1999).
6. Bromm, V. & Larson, R. B. The first stars. *Annu. Rev. Astron. Astrophys.* **42,** 79–118 (2004).
7. Rees, M. J. Origin of pregalactic microwave background. *Nature* **275,** 35–37 (1978).
8. Kashlinsky, A., Arendt, R., Gardner, J. P., Mather, J. & Moseley, S. H. Detecting population III stars through observations of near-infrared cosmic infrared background anisotropies. *Astrophys. J.* **608,** 1–9 (2004).
9. Kashlinsky, A., Mather, J. & Odenwald, S. Clustering of the diffuse infrared light from the COBE DIRBE maps. IV. Overall results and possible interpretations. Preprint (1999).
10. Salvaterra, R. & Ferrara, A. The imprint of the cosmic dark ages on the near-infrared background. *Mon. Not. R. Astron. Soc.* **339,** 973–982 (2003).
11. Magliochetti, M., Salvaterra, R. & Ferrara, A. First stars contribution to the near-infrared background fluctuations. *Mon. Not. R. Astron. Soc.* **342,** L25–L29 (2003).
12. Santos, M., Bromm, V. & Kamionkowski, M. The contribution of the first stars to the cosmic infrared background. *Mon. Not. R. Astron. Soc.* **336,** 1082–1092 (2002).
13. Cooray, A., Bock, J., Keating, B., Lange, A. & Matsumoto, T. First star signature in infrared background anisotropies. *Astrophys. J.* **606,** 611–624 (2004).
14. Kashlinsky, A. & Odenwald, S. Clustering of the diffuse infrared light from the COBE DIRBE maps. III. Power spectrum analysis and excess isotropic component of fluctuations. *Astrophys. J.* **528,** 74–95 (2000).
15. Matsumoto, T. *et al.* Infrared telescope in space observations of the near-infrared extra-galactic background light. *Astrophys. J.* **626,** 31–43 (2005).
16. Kashlinsky, A., Odenwald, S., Mather, J., Skrutskie, M. & Cutri, R. Detection of small-scale fluctuations in the near-infrared cosmic infrared background from long-exposure 2MASS fields. *Astrophys. J.* **579,** L53–L57 (2002).
17. Odenwald, S., Kashlinsky, A., Mather, J., Skrutskie, M. & Cutri, R. Analysis of the diffuse near-infrared emission from Two-Micron All-Sky Survey deep integration data: Foregrounds versus the cosmic infrared background. *Astrophys. J.* **583,** 535–550 (2003).
18. Fazio, G. G. *et al.* Number counts at $3\,\mu m < \lambda < 10\,\mu m$ from the Spitzer Space Telescope. *Astrophys. J. Suppl.* **154,** 39–43 (2004).
19. Fazio, G. G. *et al.* The Infrared Array Camera (IRAC) for the Spitzer Space Telescope. *Astrophys. J. Suppl.* **154,** 10–17 (2004).
20. Barmby, P. *et al.* Deep mid-infrared observations of Lyman break galaxies. *Astrophys. J. Suppl.* **154,** 97–102 (2004).
21. Fixsen, D. J., Moseley, S. H. & Arendt, R. G. Calibrating array detectors. *Astrophys. J. Suppl.* **128,** 651–658 (2000).
22. Högbom, J. Aperture synthesis with a non-regular distribution of interferometer baselines. *Astrophys. J. Suppl.* **15,** 417–426 (1974).
23. Kelsall, T. *et al.* The COBE Diffuse Infrared Background Experiment search for the cosmic infrared background. II. Model of the interplanetary dust cloud. *Astrophys. J.* **508,** 44–73 (1998).
24. Kaiser, N. On the spatial correlations of Abell clusters. *Astrophys. J.* **284,** L9–L12 (1984).
25. Bertin, E. & Arnouts, S. SExtractor: Software for source extraction. *Astron. Astrophys. Suppl.* **117,** 393–404 (1996).
26. Bennett, C. *et al.* First-year Wilkinson Microwave Anisotropy Probe (WMAP) observations: Preliminary maps and basic results. *Astrophys. J. Suppl.* **148,** 1–37, (2003).
27. Perlmutter, S. *et al.* Measurements of omega and lambda from 42 high-redshift supernovae. *Astrophys. J.* **517,** 565–586 (1999).
28. Efstathiou, G., Sutherland, W. J. & Maddox, S. J. The cosmological constant and cold dark matter. *Nature* **348,** 705–707 (1990).
29. Tegmark, M. *et al.* Cosmological parameters from SDSS and WMAP. *Phys. Rev. D* **69,** 103501–103527 (2004).
30. Peacock, J. & Dodds, S. J. Non-linear evolution of cosmological power spectra, 1996. *Mon. Not. R. Astron. Soc.* **280,** L19–L26 (1996).
31. Maddox, S., Efstathiou, G., Sutherland, W. & Loveday, J. Galaxy correlations on large scales. *Mon. Not. R. Astron. Soc.* **242,** 43P–47P (1990).
32. Springel, V. *et al.* Simulations of the formation, evolution and clustering of galaxies and quasars. *Nature* **435,** 629–636 (2005).
33. Oliver, S. *et al.* Angular clustering of galaxies at 3.6 microns from the Spitzer Wide-area Infrared Extragalactic (SWIRE) survey. *Astrophys. J. Suppl.* **154,** 30–34 (2004).
34. Steidel, C. *et al.* Spectroscopic identification of a protocluster at $z = 2.300$: Environmental dependence of galaxy properties at high redshift. *Astrophys. J.* **626,** 44–50 (2005).
35. Miralda-Escude, J. The dark age of the Universe. *Science* **300,** 1904–1909 (2003).
36. Kashlinsky, A. Reconstructing the spectrum of the pregalactic density field from astronomical data. *Astrophys. J.* **492,** 1–28 (1998).
37. Gautier, T. N., Boulanger, F., Perault, M. & Puget, J. L. A calculation of confusion noise due to infrared cirrus. *Astron. J.* **103,** 1313–1324 (1992).
38. Ingalls, J. G. *et al.* Structure and colors of diffuse emission in the Spitzer galactic first look survey. *Astrophys. J.* **154,** 281–285 (2004).
39. Wright, E. L. Angular power spectra of the COBE DIRBE maps. *Astrophys. J.* **496,** 1–8 (1998).
40. Eisenhardt, P. R. *et al.* The Infrared Array Camera (IRAC) shallow survey. *Astrophys. J. Suppl.* **154,** 48–53 (2004).
41. Cowie, L. L. *et al.* New insight on galaxy formation and evolution from Keck spectroscopy of the Hawaii Deep Fields. *Astron. J.* **112,** 839–864 (1996).
42. Shapley, A. E. *et al.* Ultraviolet to mid-infrared observations of star-forming galaxies at $z \sim 2$: Stellar masses and stellar populations. *Astrophys. J.* **626,** 698–722 (2005).
43. Hauser, M. G. *et al.* The COBE diffuse infrared background experiment search for the cosmic infrared background. I. Limits and detections. *Astrophys. J.* **508,** 25–43 (1998).
44. Wright, E. L. DIRBE minus 2MASS: Confirming the cosmic infrared background at 2.2 microns. *Astrophys. J.* **553,** 538–544 (2001).
45. Arendt, R. *et al.* The COBE diffuse infrared background experiment search for the cosmic infrared background. III. Separation of galactic emission from the infrared sky brightness. *Astrophys. J.* **508,** 74–105 (1998).
46. Dwek, D. & Arendt, R. A tentative detection of the cosmic infrared background at 3.5 μm from COBE/DIRBE observations. *Astrophys. J.* **508,** L9–L12 (1998).
47. Wright, E. L. & Reese, E. D. Detection of the cosmic infrared background at 2.2 and 3.5 microns using DIRBE observations. *Astrophys. J.* **545,** 43–55 (2000).
48. Gorjian, V., Wright, E. L. & Chary, R. R. Tentative detection of the cosmic infrared background at 2.2 and 3.5 microns using ground-based and space-based observations. *Astrophys. J.* **536,** 550–560 (2000).
49. Cambresy, L., Reach, W. T., Beichman, C. A. & Jarrett, T. H. The cosmic infrared background at 1.25 and 2.2 microns using DIRBE and 2MASS: A contribution not due to galaxies? *Astrophys. J.* **555,** 563–571 (2001).


**Supplementary Information** is linked to the online version of the paper at www.nature.com/nature.

**Acknowledgements** We thank G. Fazio for access to the IRAC Deep Survey data and D. Fixsen and G. Hinshaw for comments on drafts of this paper. This Article reports work supported by the National Science Foundation, and which is based on observations made with the Spitzer Space Telescope (this telescope is operated by the Jet Propulsion Laboratory, California Institute of Technology, under a contract with NASA). Support for this work was also provided by NASA through an award issued by JPL/Caltech.

**Author Contributions** A.K. is responsible for the idea, clipping the maps, power spectrum and correlation analyses, evaluating the extragalactic contributions and writing the paper. R.G.A. is responsible for the images for analysis, providing the model of the resolved sources with the IRAC PSF, and evaluating systematics, instrument, and zodiacal and cirrus contributions. J.M. and S.H.M. developed analysis strategy and searched for alternative explanations for the fluctuations. All authors provided critical review of the analysis techniques, results and manuscript.

**Author Information** Reprints and permissions information is available at npg.nature.com/reprintsandpermissions. The authors declare no competing financial interests. Correspondence and requests for materials should be addressed to A.K. (kashlinsky@stars.gsfc.nasa.gov).